EUROPEAN FUSION DEVELOPMENT AGREEMENT

EFDA–JET–PR(03)48

D. Testa, A. Fasoli, D. Borba, M.de Baar, M. Bigi, J. Brzozowski, P.de Vries
and JET EFDA contributors

Alfvén Mode Stability and Wave-Particle Interaction in the JET Tokamak: Prospects for Scenario Development and Control Schemes in Burning Plasma Experiment

Alfvén Mode Stability and Wave-Particle Interaction in the JET Tokamak: Prospects for Scenario Development and Control Schemes in Burning Plasma Experiment

D. Testa[1], A. Fasoli[1,2], D. Borba[3], M.de Baar[4], M. Bigi[5], J. Brzozowski[6], P.de Vries[5] and JET EFDA contributors*

[1]*CRPP, Association EURATOM – Confédération Suisse, EPFL, Lausanne, Switzerland*
[2]*Plasma Science and Fusion Center, Massachusetts Institute of Technology, Boston, USA*
[3]*Associacão EURATOM/IST, Portugal; and EDFA – CSU, Culham Science Centre, UK*
[4]*FOM – Instituut Voor Plasmafysica, Rijnhuizen, The Netherlands*
[5]*Euratom/UKAEA Fusion Association, Culham Science Centre, Abingdon, UK*
[6]*NADA VR – Euratom Association, Royal Institute of Technology, Stockholm, Sweden*
** See annex of J. Pamela et al, "Overview of Recent JET Results and Future Perspectives", Fusion Energy 2000 (Proc. 18th Int. Conf. Sorrento, 2000), IAEA, Vienna (2001).*

Preprint of Paper to be submitted for publication in
Plasma Physics and Controlled Fusion

ABSTRACT.

We have investigated the effect of different Ion Cyclotron Resonance Frequency (ICRF) heating schemes, of error field modes, of the plasma shape and edge magnetic shear, and of the ion ∇B-drift direction on the stability of Alfvén Eigenmodes (AEs). The use of multi-frequency or 2^{nd} harmonic minority ICRF heating at high plasma density gives rise to a lower fast ion pressure gradient in the plasma core and to a reduced mode activity in the Alfvén frequency range. Externally excited low-amplitude error fields lead to a much larger AE instability threshold, which we attribute to a moderate radial redistribution of the fast ions. The edge plasma shape has a clear stabilising effect on high-n, radially localised AEs. The damping rate of n=1 Toroidal AEs is a factor three higher when the ion ∇ B-drift is directed towards the divertor. These results represent a useful step towards the extrapolation of current scenarios to the inclusion of fusion-born alpha particles in ITER, with possible application for feedback control schemes for the various ITER operating regimes.

1. INTRODUCTION.

Controlling the interaction between fusion-born alpha particles (α's) and modes in the Alfvén frequency range is a crucial issue for ITER operation [1,2], as these modes can be driven unstable by the slowing-down α's up to amplitudes at which they could cause rapid radial transport of the α's themselves [3]. Furthermore, interaction between the α's and modes that affect the topology of the magnetic surfaces, such as sawteeth, could lead to a fast core-edge radial redistribution of the α's. The loss of a confinement can then affect the burn process and possibly cause damage to the first wall. It is therefore very important to assess the regimes under which such losses can occur.

This topic is studied in JET [4] using direct measurements of the fast ion distribution function $f_{FAST}(E,r,t)$ and of the modes' instability threshold, amplitude and damping. The typical operating scenarios involve ions driven to MeV energies by Ion Cyclotron Resonance Frequency (ICRF) heating, with the most common one being 1^{st} harmonic ICRF heating of the minority hydrogen population in deuterium plasmas [5]. In this H(D) minority heating scheme, the fast ion tail can reach a perpendicular temperature $T_{\perp FAST} \approx 500$keV in the plasma core, much larger than the electron and ion temperatures, $T_e \approx T_i \approx$ 10keV. The fast ion energy distribution function is anisotropic, and the ratio between the parallel and perpendicular fast ion temperature is typically $T_{\|FAST}/T_{\perp FAST} \approx 0.1$. The shape of the ICRF power deposition profile can be used to vary the normalised fast ion pressure $\beta_{FAST} = 2\mu_0 p_{FAST}/B^2$ (here μ_0 is the vacuum magnetic permeability, p_{FAST} the fast ion pressure and B the plasma magnetic field). The local peaking of β_{FAST} can be controlled with the phasing of the ICRF antennas and by spreading the power deposition profile using multi-frequency heating. Thus, despite the anisotropy of their energy distribution function, these ICRF-driven MeV-energy fast ions provide a good simulation tool for the fusion-born a's in ITER.

In this paper we address with a number of different JET examples the important question of the interplay between the fast ion populations and the fast ion driven modes. Specifically, in the long-term ITER perspective, we consider possible ways to control and/or prevent, by tailoring the α's

radial profile, the radial transport of the α's from the plasma core to the edge that may be caused by α-driven modes. The aim of this study is two-fold. First, it is paramount to move from the separate knowledge of the modes and the fast ion distribution function to self-consistent extrapolations for the integrated scenarios foreseen for the various ITER operating regimes. Second, the results of this work can be used to study possible feedback control schemes for the modes and the fast ions.

Fast particle redistribution can be caused either by a global mode occupying the entire plasma cross-section, or by a sequence of radially localised modes extending from the plasma core to the edge. Both classes of modes are well represented in JET (and ITER) by Alfvén Eigenmodes (AEs) [6]. AEs with low toroidal mode number (n) are global modes, whereas high-n AEs are typically radially localised modes. AEs can be driven unstable in ITER by a strong peaking of the a pressure gradient, and are regularly observed in JET when the drive for the modes, $\gamma_{DRIVE} \propto \nabla\beta_{FAST}$, exceeds the sum of all the various damping terms, γ_{DAMP}. Hence combining direct measurements of the modes and of the fast ion distribution function provides the necessary information to study in details the wave-particle interaction mechanisms [7].

For both low-n and high-n AEs, it is clear that creating a strong energy sink mechanism for the modes at the plasma edge could in principle be sufficient to prevent significant a losses. For the case of radially localised modes, it may also be possible to break-up such sequence inside the plasma by modifying the drive for some of these modes via a local reduction of $\nabla\beta_{FAST}$. It is also clear that the radial profile of the fusion-born α's distribution function will need to be optimised in order to achieve a high fusion yield and sustain the burn process. Hence, a more subtle question in terms of possible control schemes is the interaction between the modes and the fuel ions. In this respect, a controlled radial redistribution of the fuel ions and/or the α's themselves could also be beneficial to reduce the peaking of the α pressure gradient and prevent high-amplitude instabilities that may affect the global plasma transport properties and the α confinement.

The following Sections present different examples of how to affect the AE instability threshold and fast particle pressure gradient in plasmas with a monotonic safety factor profile q(r). Specifically, in Sections 2 to 4 we present the results of different experiments where the AE stability is significantly modified by affecting f_{FAST} (E,r,t), hence γ_{DRIVE}. Another tool to affect the AE stability is acting on γ_{DAMP}, and two examples are presented in Sections 5 and 6. In Section 2 we consider the role of multi-frequency ICRF heating to spread the power deposition profile and locally reduce $\nabla\beta_{FAST}$. In Section 3 we study the AE stability for 2nd harmonic H(D) ICRF heating as function of the plasma density. Section 4 discusses the effect of low-amplitude error field modes in causing a local redistribution of the ICRF-driven MeV energy ions around the q=2 surface. In Section 5 we analyse the effect of the edge plasma shape and magnetic shear in determining the instability threshold and non-linear behaviour of Toroidal AEs (TAEs) with intermediate n's. In Section 6 we consider the dependence of the damping rate for n=1 TAEs on the ion ∇B-drift direction. Finally, in Section 7 we present our conclusions and discuss possible application of these JET results to ITER plasmas.

2. THE ROLE OF MULTI-FREQUENCY 1ST HARMONIC H(D) ICRF HEATING ON THE AE STABILITY.

The aim of this Section is to assess differences between single-frequency (monochromatic) and multi-frequency (polychromatic) ICRF operation in JET for similar background plasma parameters, using magnetic fluctuation measurements and direct measurements of the minority hydrogen energy distribution function $f_{HFAST}(E,t)$ and the perpendicular tail temperature $T_{\perp HFAST}$ in the plasma core. The fast ion distribution function and perpendicular temperature are measured in JET using a high energy Neutral Particle Analyser (NPA) [8-10]. The NPA is of the E||B type, and views the plasma vertically with its line-of-sight intersecting the plasma midplane at R_{NPA}=3.07m, very close to the magnetic axis, R_{MAG}~3m. The line-of-sight geometry determines that only ions with $\upsilon_{\perp}/\upsilon_{\|}\geq 200$ can be detected by the NPA. There are eight energy channels in the range $0.2\leq E(MeV)\leq 3.5$, with common charge and mass selection, thus only one ion species can be measured at any one time. These fast ions escape the plasma after having been neutralised in the plasma core via electron recombination and charge-exchange reactions with background impurity ions and thermal and high-energy neutral atoms, such as those provided by Neutral Beam Injection (NBI) [11].

Earlier measurements of $f_{HFAST}(E)$ have shown that, for the same level of P_{ICRF}, 1st harmonic H(D) polychromatic heating produces a lower $T_{\perp HFAST}$ than monochromatic heating [12,13]. Moreover, for polychromatic heating a more peaked electron temperature profile $T_e(r)$, and an increase in the central ion temperature T_{i0}, or the same T_{i0} for a much higher central electron density n_{e0}, were also observed [14]. These initial results give rise to favourable extrapolations for ITER operation but need to be further verified in plasma configurations and operating regimes far better matched than those used in the original studies. Furthermore, polychromatic operation will become more relevant in JET when the ITER-like antenna becomes operational during 2005, thus increasing the available ICRF power and providing for more direct ITER extrapolations.

In the case of monochromatic heating, the ICRF power deposition profile is peaked on the magnetic axis, $R_{ABS}\approx 3m\approx R_{MAG}$, and can be well approximated with a gaussian shape with half-width at half-maximum of the order of the Doppler shift of the resonance [10,12,13], $\sigma_{ABS}\approx k_{\|}v_{th\|H}/\Omega_H$. Here $k_{\|}$ is the parallel wavenumber, $v_{th\|H}\approx (2T_{\|HFAST}/m_H)^{1/2}$ is the parallel thermal velocity of the MeV-energy hydrogen ions, with $T_{\|HFAST}\approx T_{\perp HFAST}/10$, and Ω_H is the 1st harmonic hydrogen cyclotron angular frequency, giving $\sigma_{ABS}\approx 25cm$. Using a similar argument for polychromatic heating, the total power deposition profile is given by the convolution of those obtained for each individual frequency, all with different R_{ABS}. The width of the power deposition profile can then be approximated by the geometric mean of the sum of the Doppler width and the position of each R_{ABS}:

$$\sigma_{ABS}=\left\{\sum_j\left[\sigma_{ABS,j}^2+(R_{ABS,j}-R_{MAG})^2\right]\right\}^{1/2}, \qquad (1)$$

giving the value of $\sigma_{ABS}\approx 50cm$ for the cases considered here.

As typical examples of polychromatic and monochromatic heating we consider Pulse No's: 57296

and 57298, respectively. Figures 1a and 1b show that the measured $T_{\perp HFAST}$ is slightly higher in Pulse No: 57298 than in Pulse No:57296, with a very similar time evolution. This difference, although small, is still significant since it is outside the error bars on the measurements of $T_{\perp HFAST}$ and $f_{HFAST}(E)$ for these cases. Notice also the slightly higher T_{e0} in Pulse No: 57298 for t = (7.5÷9)sec, consistent with the $T_{\perp HFAST}$ measurements. Figure 2 shows the comparison between $f_{HFAST}(E)$ in Pulse No's: 57296 and 57298 at various time points of interest. The markers and the lines indicate respectively the measured and fitted $\log_{10}(f_{HFAST}(E))$. The absolute value of $f_{HFAST}(E)$ is approximately 25% higher in Pulse No: 57296 than in Pulse No: 57298, indicating a larger density ratio n_{HFAST}/n_e in the plasma core for Pulse No: 57296, as shown in Fig.3. We note as well that the relative difference $\Delta f_{HFAST}(E)/f_{HFAST}(E)$ is clearly larger at lower energies during the steady-state phase. This further indicates that polychromatic heating is less effective than monochromatic heating in creating a high-energy tail in the minority ion distribution function in the plasma core.

The measurement of the mode activity in the Alfvén frequency range confirms this conclusion, as shown in Figs.4a and 4b. The mode amplitude ($|\delta B|$), the toroidal and poloidal (m) mode numbers are measured with pick-up coils located at the plasma edge using the technique described in [15]. The mode numbers are obtained with a linear fit of the measured phase difference between adjacent probes as a function of the probes' angle in the toroidal (poloidal) direction, $\Delta phase = constant + n(m) \times \Delta angle$. To obtain the poloidal mode numbers, the physical position of the pick-up coils, mounted on the vessel, has to be corrected for the curvature of the poloidal magnetic field lines at the mode radial location, the so-called *thetastar correction* of the probe angle [15]. The uncertainty on the calculated mode numbers comes mainly from the errors on the calibration of the frequency dependence of the phase response for the various probes. The error on the inferred m's is larger than that on the n's, since it also depends on the accuracy of the equilibrium reconstruction at the mode radial location. We estimate that for the plasma configurations reported here the error on the m's is approximately 50% larger than that on the n's, typically $|\Delta n/n| \approx 0.1$ and $|\Delta m/m| \approx 0.15$. The position of radially localised modes can be inferred using three methods [16]: first, from the measured mode numbers by comparison with the calculated eigenfunction radial structure; second, using the cross-correlation between edge magnetics and internal (electron cyclotron emission and reflectometry) measurements; and third, from the measured toroidal rotation profile using the Doppler shift in the frequency of modes with different n's.

During the ICRF heating phase, in Pulse No: 57296 we observe a TAE with (dominant at the plasma edge) poloidal and toroidal mode numbers m/n=8/4 and a m/n=9(8?)/3 Ellipticity-induced AE (EAE) around 200kHz and 400kHz, respectively. On the other hand, for Pulse No: 57298 no EAEs are detected and two m/n=9/4 and m/n=11/5 TAEs with significantly higher amplitude ($|\delta B|$) are detected around 200kHz. From their toroidal and poloidal mode numbers, we infer that the TAEs are located around the q-surface $q_{TAE} \approx (2m+1)/2n \approx 2$ and the EAEs around the $q_{EAE} \approx (m+1)/n \approx 3$ surface, indicating that they are localised further off-axis. The q-profile is determined using a magnetic reconstruction of the equilibrium constrained by motional Stark effect and polarimetry measurements.

These values are confirmed by the position of the sawtooth inversion radius, as deduced from the electron cyclotron emission measurements of the electron temperature. Thus the presence/absence of the q=3 EAEs and the lower amplitude of the q=2 TAEs clearly confirms that the $f_{HFAST}(E,r)$ radial profile is broader and less peaked on-axis for polychromatic than for monochromatic heating.

3. THE ROLE OF 2ND HARMONIC H(D) ICRF HEATING AT HIGH PLASMA DENSITY ON THE AE STABILITY.

Operation at high density is required to reach the burning plasma regimes in ITER [1,2]. The DT fusion cross section has a broad peak around $E_D \approx E_T \approx 70$keV/amu, and the temperature of the bulk plasma ions has to reach similar values in order to maximise the fusion yield. Therefore, in view of possible extrapolations of the minority ICRF heating schemes used in JET to the heating of the fuel ions in ITER, it becomes important to study the stability of fast ion driven AEs as a function of the plasma density for otherwise similar plasma conditions. To this aim, a series of experiments were performed using the 2nd harmonic H(D) ICRF heating scheme. The ICRF power $P_{ICRF} = 5.2$MW and resonance position $R_{ABS} \approx 3.07$m, the electron temperature profile (with $T_{e0} \approx 3.5$keV) and the shape of the electron density profile were very well matched between the discharges analysed here, allowing for a direct comparison of $T_{\perp HFAST}$ as a function of the electron density in the plasma core n_{e0}. As representative cases for the low and high n_{e0} scenario in the steady-state conditions achieved during the P_{ICRF} flat-top phase, we consider here Pulse No:57225 (with $n_{e0} \approx 3\times10^{19}m^{-3}$) and Pulse No: 57226 (with $n_{e0} \approx 4\times10^{19}m^{-3}$), respectively. The volume-averaged density ratio $\langle n_H/n_e \rangle$ is larger in Pulse No: 57225 than in Pulse No: 57226, $\langle n_H/n_e \rangle \approx 2\%$ compared to $\langle n_H/n_e \rangle \approx 1.3\%$, due to a different recycling from the wall. Thus the absolute volume-averaged density of the minority hydrogen population is very similar for these two discharges, $\langle n_H \rangle \approx 5\times10^{17}m^{-3}$, which gives rise to a similar ICRF power-per-particle. Therefore all differences in the AE stability can be associated to the effect of n_{e0} on $T_{\perp HFAST}$ and γ_{DAMP}.

Figures 5a and 5b show an almost double $T_{\perp HFAST}$ at low plasma density, $T_{\perp HFAST} \approx 200$keV in Pulse No: 57225 compared to $T_{\perp HFAST} \approx 120$keV in Pulse No: 57226. The error in the $T_{\perp HFAST}$ measurements is of the order of $|\Delta T/T| \approx 15\%$ in Pulse No: 57225 and $|\Delta T/T| \approx 25\%$ in Pulse No: 57226. The larger $|\Delta T/T|$ in Pulse No: 57226 is due to a much lower count rate for $E_H > 1$MeV. It is also important to note that for similar background plasma parameters and P_{ICRF}, we typically observe a much higher $T_{\perp HFAST} > 300$keV for 1st harmonic H(D) heating. This result is consistent with the fact that the efficiency of 2nd harmonic heating depends essentially on the presence of a seed population of non-thermal ions with Larmor radius of the order of the perpendicular wavelength of the ICRF wavefield, $k_\perp \rho_i \rightarrow 1$ [12,13].

Figure 6 shows the comparison between $f_{HFAST}(E)$ in Pulse No's: 57225 and 57226 at various time points of interest. The markers and the lines indicate the measured and fitted $\log_{10}(f_{HFAST}(E))$, respectively. We note that $f_{HFAST}(E)$ is higher in Pulse No: 57225 than in Pulse No: 57226 at all energies, and that the count rate for energies $E_H > 1$MeV is very low, hence causing a larger uncertainty

in the results. The absolute value of $f_{HFAST}(E)$ is 5÷10% higher in Pulse No: 57225 than in Pulse No: 57226 for energies up to E_H=0.765MeV, and more than 50% higher for E_H>0.9MeV. This indicates a larger density ratio n_{HFAST}/n_e in the plasma core and a much larger tail energy content for Pulse No: 57225, as shown in Fig.7. The vertical lines indicate the time of two sawteeth in Pulse No: 57225, which cause a large depletion in $f_{HFAST}(E)$ for E>1.3MeV.

As shown in Fig.8a, during the ICRF heating phase of Pulse No: 57225 we observe m/n=(7-12)/(5-8) TAEs in the frequency range 120≤f(kHz)≤140 for P_{ICRF}>3MW. From the toroidal mode numbers and the Doppler shift in the frequency of AEs with different n's, we infer that the modes are located around r/a ≈ 0.4, and that the toroidal rotation frequency at the mode location is $f_{\phi ROT}(r/a \approx 0.4) \approx$ 7kHz. Figure 8b shows that in Pulse No:57226 m/n=(8-12)/(6-8) TAEs are excited at a higher power P_{ICRF}>3.6MW at a lower frequency 120≤f(kHz)≤130 due to the higher plasma density. The n=5 mode (and the n=8 mode to some extent) is very weak ($|\delta B| \approx 10^{-6.4}$T in Pulse No: 57226 compared to $|\delta B| \approx 10^{-5.8}$T in Pulse No: 57225) and intermittent, almost undetectable in the spectrum, thus indicating a lower drive at the mode location. The toroidal rotation frequency is $f_{\phi ROT}(r/a \approx 0.4) \approx$ 5kHz at the mode location, lower than in Pulse No: 57225 due to the higher n_{e0}, consistent with a lower β_{HFAST} [17,18]. These observations, and specifically the lower fast ion count rate in the higher energy channels of the NPA (E_H>1MeV), the weaker n=5 mode and the reduction in the toroidal rotation frequency at the mode location, clearly confirm the lower $T_{\perp HFAST}$ and β_{HFAST} at higher plasma density for the 2nd harmonic H(D) ICRF heating scheme.

4. THE ROLE OF ERROR FIELDS ON THE AE STABILITY.

The AE stability can be affected by the onset of other instabilities that modify the AE drive by causing a redistribution of the fast ions. For the typical JET operating scenarios, two examples of these observations are the rapid density perturbation associated with pellet injection [19], and the appearance of a q=1 magnetic island associated with a sawtooth crash [7]. Here we investigate the effect on the fast particle population, hence the AE drive, of externally induced error fields locking to the q=2 surface and generating a magnetic island. The interest for this kind of experiment stems from the fact that an ad-hoc radial redistribution of the fast ions could in principle be beneficial in locally reducing $\nabla\beta_{FAST}$, hence the drive for AEs or Energetic Particle Modes [20]. Such controlled radial redistribution may prevent these modes to reach high amplitudes, which could lead, in turn, to a very rapid fast ion transport from the plasma core to the edge that could cause significant fast ion losses in certain scenarios [21]. In the absence of radially resolved measurements of $f_{FAST}(E,t)$, the onset and the disappearance of AEs localised at different radial positions can then be used to provide evidence for the fast ion redistribution [7].

Figure 9a shows the magnetic fluctuation spectrum for a discharge where a q=2 error field was applied (Pulse No: 59343), and Fig.9b shows the reference case without error field for very similar plasma parameters (Pulse No: 59344). In both cases, the q=2 and q=3 surfaces are located around $(r/a)_{q=2} \approx 0.55$ and $(r/a)_{q=3} \approx 0.7$. The in-vessel saddle coils were used during the time interval

t_{EF}=19÷21.5sec to apply this error field, with maximum current $I_{SC} \approx 3$kA. The plasma density is fairly low, $n_{e0}<2\times10^{19}m^{-3}$, giving rise to a long decay time for this externally induced q=2 island, $\tau_{EF}>3$sec. In both cases we observe EAEs associated with the q=3 surface, although their behaviour is different. In the presence of the error fields the EAEs are almost continuous at frequencies around $f_{EAE} \approx 400$kHz, whereas without the error fields they are rapidly chirping down, a commonly observed feature. On the other hand, with the error fields we do not observe TAEs in the frequency range $f_{TAE} \approx 150 \div 200$kHz, as we do without the error fields. This indicates that the drive for these modes has been removed by the error fields and the induced magnetic island around the q=2 surface, with a much weaker effect around the q=3 surface. Figures 10a and 10b show the measurement of the mode amplitude for the n=4 TAE and n=4 EAE observed in these two discharges as function of P_{ICRF}. Without the error fields, the n=4 TAE becomes unstable at $P_{ICRF} \gtrsim 3$MW, and during the ICRF flat-top phase reaches the amplitude at the plasma edge $|\delta B|_{TAE} \approx 1.3\times10^{-5}$T. The only difference observed for the n=4 EAE when the error fields are applied is the much higher excitation threshold, $P_{ICRF} \approx 1.1$MW without error fields compared to $P_{ICRF} \gtrsim 2$MW with error fields, thus indicating that a larger drive is required in this case. During the ICRF flat-top phase, the mode reaches in both cases the amplitude at the plasma edge $|\delta B|_{EAE} \approx 1.4\times10^{-5}$T, very similar to $|\delta B|_{TAE}$.

Figure 11 shows the comparison between $f_{HFAST}(E)$ in Pulse No's: 59343 and 59344 at various time points of interest. The markers and the lines indicate respectively the measured and fitted $\log_{10}(f_{HFAST}(E))$. We note that $f_{HFAST}(E)$ is approximately 40% higher without error fields, indicating a larger n_{HFAST} in the plasma core. The measured $T_{\perp HFAST}$ in the plasma core is approximately 20% higher in the presence of the error fields due of a lower $<n_H>$, $<n_H> \approx 5\times10^{17}m^{-3}$ in Pulse No: 59343 and $<n_H> \approx 9\times10^{17}m^{-3}$ in Pulse No: 59344. Considering now the Stix's model [22] to infer the dependence of $T_{\perp HFAST}$ on n_{HFAST}, we have $T_{\perp HFAST} = T_e + (\rho_{ABS}\,\tau_{SD})/3n_{HFAST}$, where τ_{ABS} is the absorbed power density and τ_{SD} the fast ion slowing-down time. Hence we would expect $T_{\perp HFAST}$ to be ~(9/5) larger in the plasma core for the same P_{ICRF} due to the lower $<n_H>$ if the presence of the error fields had no effect on it, whereas we only measure a ~20% increase. This data then indicates a much lower β_{FAST} in the plasma core, confirming the indication obtained with the measurements of the TAE and EAE mode amplitude.

5. THE EFFECT OF THE EDGE PLASMA SHAPE AND MAGNETIC SHEAR ON THE HIGH-N TAE STABILITY

In the previous three sections we have presented different examples of JET experiments where the AE stability was modified by affecting $f_{FAST}(E,r,t)$, hence γ_{DRIVE}. Now we turn our attention to the complementary line of action, i.e. to possible ways of affecting the AE stability by acting on γ_{DAMP}. The effect of the edge plasma shape and magnetic shear on the damping rate γ/ω of low-n AEs in discharges with monotonic q-profile has been presented in [23], where it was found that for radially extended n=1 TAEs γ/ω increases strongly with increasing edge magnetic shear $s=(r/q)(dq/dr)$, elongation (κ_{95}) and triangularity (δ). Here we consider the role of these parameters on the stability of

radially localised n=3-10 TAEs excited by resonant NBI ions, with $\upsilon_{\|NBI} \approx \upsilon_A = B/(\mu_0\rho)^{1/2}$ (here ρ is the plasma mass density). These modes are expected to be more easily destabilised in ITER by the fast ion populations than low-n TAEs in JET for similar background plasma parameters, due to the dependence of the most unstable n's on the normalised Larmor radius [24].

As representative of the edge shape and magnetic shear in the ITER standard scenarios [2], here we consider plasmas with a monotonic q-profile, $q_0 = q(r/a = 0) \approx 0.8$ and $q_{95} = q(r/a = 0.95) \approx 3.0 \div 3.2$. Figures 12a and 12b show the comparison between plasmas with low and high edge magnetic shear (limiter and X-point configuration, respectively). For the X-point scenario, a ramp in the NBI heating power (P_{NBI}) is used to determine the TAE instability threshold. In JET the NBI ions are injected at a nominal birth energy $E_b = 80$keV and $E_b = 140$keV, and the 1/2 and 1/3 components contribute to approximately 30% of the total number of NBI ions injected. For similar background plasmas, we find that one needs approximately 50% more NBI power, $P_{NBI} = 8$MW compared to $P_{NBI} = 5.3$MW, and NBI fast ions with parallel velocity much closer to the resonant velocity, $\max(\upsilon_{\|NBI}) \approx 0.95\upsilon_A$ compared to $\max(\upsilon_{\|NBI}) \approx 0.8\upsilon_A$ because of a slightly different plasma density profile, to destabilise TAEs with intermediate n's in plasmas with high edge magnetic shear than in plasmas with low edge magnetic shear. The non-linear behaviour of TAEs with intermediate n's is also modified by the edge magnetic shear, as shown in Fig.13a for Pulse No: 60897 (high-s), and Fig.13b for Pulse No: 60903 (low-s). Here we consider TAEs, located around $(r/a)_{TAE} \approx 0.6$, driven by super-alfvénic NBI ions with very similar resonant velocity, $v_{\|NBI} \approx 1.05v_A$. In the high-s case we observe almost continuous n = 4÷7 TAEs at $P_{NBI} = 7.2$MW, whereas for the low-s case bursting n = 5÷7 TAEs become already unstable at $P_{NBI} = 5.6$MW. These results confirm the measurements on the stabilising effect of edge magnetic shear for low-n TAEs in plasmas with monotonic q-profiles, although this effect appears to be weaker for radially localised n = 4÷8 TAEs than for radially extended n = 1÷2 TAEs. They also motivate further experimental work to determine more accurately the scaling of the NBI power threshold as function of the velocity ratio $\max(\upsilon_{\|NBI})/\upsilon_A$.

6. THE EFFECT OF THE ION ∇B-DRIFT DIRECTION ON THE DAMPING RATE OF N=1 TAES

The direction of the ion ∇B-drift is an important parameter in determining the accessibility conditions for the high-confinement regime known as H-mode [25]. There is clear experimental evidence that the H-mode regime is obtained at a lower input power level (typically a factor two) when the ion ∇B-drift is directed towards the divertor than when it is in the opposite direction [26]. However, recent JET data indicate that the H-mode power threshold is similar for the two ion ∇B-drift directions across a range of magnetic field B=1.2-3.0T and low electron density at the plasma edge, $n_e(\text{edge}) < 2\times10^{19}\text{m}^{-3}$ [27]. Thus it is important to study the implications of this fundamental choice for ITER operation on the value of the background plasma damping of low-n TAEs.

Figures 14a and 14b show the main plasma parameters and γ/ω for n = 1 TAEs in two similar discharges with the ion ∇B-drift directed towards the divertor (named as B+ in the figure, Pulse No:

52196) and away from the divertor (B-, #59668). The mode frequency, damping rate and amplitude are obtained for low-n AEs through synchronous detection of the plasma response to a low amplitude perturbation driven by the saddle coils, typically with $I_{SC} \approx 10A$ [28]. The low edge magnetic shear phase of the discharges and similar plasma conditions were chosen, with the plasma kept in L-mode. However, certain differences in the density and temperature profiles were present due to slightly different breakdown scenarios. The damping rate of n=1 TAEs with similar frequency and radial location (defined as the position of the peak $|\delta B|$, obtained from synchronous detection of electron cyclotron emission and reflectometry measurements) is approximately a factor three higher for the case of ion ∇B-drift directed away from the divertor. To eliminate the possible effect on γ/ω of the different density and temperature profiles, we have compared various discharges with the ion ∇B-drift directed towards the divertor and the same q-profile, edge magnetic shear and shape (κ_{95} and δ), but with slightly different edge density and temperature profile as in the [B+,B-] comparison reported here. This analysis has led us to estimate that the underlying differences in the density and temperature profiles in the discharges considered here could account for a ~30% variation in γ/ω. Therefore, this data clearly suggests that the *favourable* ion ∇B-drift direction would correspond to a much lower instability threshold for low-n TAEs in ITER.

Another interest for the measurements reported here stems from the fact that the ∇B-drift terms are among the terms that are not present in fluid models, but which can be included in gyro-kinetic models of the TAE wavefield [29]. Hence the significant difference in the observed damping rate for different ion ∇B-drift directions could be used to test the prediction of these different classes of modelling, and motivates further theoretical developments.

CONCLUSIONS AND IMPLICATIONS FOR ITER.

The results presented here clearly point to the need of integrated modelling of the current operating scenarios for extrapolation to ITER, so as to consider in a self-consistent way the properties of the bulk plasma and of the fast ion populations. A specific application is the study and development of operational methods for sustaining the driven burn process through tailoring of the radial profile of the α's distribution function and real-time control of the Alfvén mode stability. First, this can be achieved via scenario optimisation. In this respect, the measurement of the dependence of γ/ω for n=1 TAEs on the ion ∇B-drift direction clearly indicates that fundamental choices on the ITER operating scenario may have unexpected effects on the AE stability limits and need to be considered in more depth in the scenario modelling. Second, an obvious method for controlling the AE stability would be affecting the damping in real-time, for instance via minor modifications of certain plasma parameters, such as the edge plasma shape and magnetic shear, as shown in Section 5.

The results presented in Sections 2 and 3 show that the use of different ICRF heating schemes has a clear impact on the AE stability limits in JET through tailoring of the radial profile of $f_{FAST}(E,r,t)$. Specifically, polychromatic ICRF heating reduces the peaking of β_{FAST} by spreading the power deposition profile, thus increasing the TAE instability threshold, and at the same time it gives rise to a

lower T_{FAST}. This effect has, on one hand, clear favourable implications for operation in the start-up phase of ITER plasmas since the lower T_{FAST} could now approach the critical temperature T_{CRIT} $\approx 15T_e$ at which the fast ions preferentially heat the bulk (fuel) ions through collisions [22]. On the other hand, electron heating is reduced, which could have negative implications on current drive schemes requiring a high T_e to achieve a higher efficiency, such as Lower Hybrid waves. Similarly, the use of 2nd harmonic minority ICRF heating at higher plasma density reduces T_{FAST}, but gives rise as well to a lower fast ion driven plasma rotation in the plasma core. This effect, in the absence of direct momentum input from NBI, may in turn have negative implications for the stability of current and pressure driven modes, such as internal [30] and external [31] kinks and for turbulence control and transition to high confinement regimes through sheared flow generation [32].

The results presented in Section 4 clearly indicate that a controlled redistribution of the α's can be beneficial for the stability of AEs with intermediate mode numbers via a reduction of the peaking of their pressure profile. Such redistribution can be triggered by resonant wave-particle diffusion in phase space, or by modes locally affecting the magnetic topology, thus giving rise to scattering of particles. This mechanism is experimentally simulated in JET during hydrogen minority ICRF heating by using the internal saddle coils to produce error fields that couple to the $q = 2$ surface. This scheme gives rise to significant modifications of the radial profile of $f_{FAST}(E,r,t)$ and reduces $\nabla\beta_{FAST}$ at the q=2 surface, hence affecting the drive for TAEs with intermediate n's.

Following up from the measurement of the dependence of the damping rate of low-n TAEs on the edge shape and magnetic shear, we have measured the P_{NBI} excitation threshold for $n = 3 \div 8$ TAEs in limiter and X-point configuration. We find that it is approximately twice as large in the case of high edge magnetic shear. Hence the edge shape is a clear tool to control the stability of AEs, both for radially extended low-n modes and radially localised high-n modes.

Considering now possible applications to ITER, it is important to point out that the use of different ICRF heating schemes is a rather indirect control tool for the α's, since the main effect would be on the fuel ions (deuterium and tritium) and not on the fusion born α's themselves. In this respect, the active excitation of modes capable of causing a controlled radial redistribution of the α's to prevent excessive peaking of their pressure gradient seems a more promising tool. In the work presented here we have shown the use of error field modes. Other possible candidates are AEs excited using in-vessel antennas or ICRF beatwaves at the appropriate resonant frequency. Similarly, the use of the edge shape to control in real-time the TAE stability has to be considered together with the operational needs for ITER, which will specify a certain range for the elongation and triangularity at the plasma edge. A proof-of-principle experiment is now planned in JET, where the real-time measurement of the damping rate of $n = 1$ TAEs will be used for feedback control of the current waveform in the plasma shaping coils.

From the experimental point-of-view, it is clear that to make more detailed and quantitative analysis of the possible fast ion redistribution caused by wave-particle interaction and mode activity, one needs radially resolved measurements of $f_{FAST}(E,r,t)$ with ~10 millisecond time resolutions, which are

lacking at the moment in JET. From the theoretical and modelling point of view, there is now a considerable wealth of information available on fast ions and mode activity from ITER-relevant experiments, from which extrapolations to ITER can be made. On the other hand, we lack self-consistent integrated scenario and transport simulations which explicitly include the detailed behaviour of the fast ion populations and their interaction with fast ion driven modes. In this respect, detailed comparisons of the measurements presented here with available theoretical models are foreseen as future work, with a view to providing suitable extrapolation for ITER.

ACKNOWLEDGEMENTS

The authors would like to acknowledge the contribution of the whole JET experimental team, and in particular Y.Andrew, C.Giroud, N.Hawkes, M.Mantsinen and S.D.Pinches.
This work has been conducted under the European Fusion Development Agreement. D.Testa and A.Fasoli were partly supported by the Fond National Suisse pour la Recherche Scientifique, Grant 620-062924, and by the DoE contract No. DE-FG02-99ER54563.

REFERENCES

[1]. R.Aymar et al., Plasma Phys. Controlled Fusion **44** (2002), 519.
[2]. ITER Physics Basis Editors, Nucl. Fusion **39** (1999), 2137; 2004 issue, in preparation.
[3]. K.Wong, Plasma Phys. Controlled Fusion **41** (1999), R1.
[4]. J.Wesson, Tokamaks, 2nd edition (Oxford Science Publication, Oxford, UK, 1997), p.581.
[5]. M.Mantsinen et al., Plasma Phys. Control. Fusion **41** (1999), 843.
[6]. C.Cheng et al., Ann. Phys. **161** (1985), 21.
[7]. A.Fasoli et al., Plasma Phys. Control. Fusion **44** (2002), 159.
[8]. A.Korotkov, A.Gondhalekar, 21st European Physical Society Conference on Controlled Fusion and Plasma Physics, Europhysics Conference Abstract 18-B(1994), I-266.
[9]. K.McClements et al., Nucl. Fusion **37** (1997), 473.
[10]. D.Testa, A.Gondhalekar, Nucl. Fusion **40** (2000), 975.
[11]. A.Korotkov et al., Nucl. Fusion **37** (1997), 35.
[12]. D.Testa et al., Phys. Plasmas **6** (1999), 3489.
[13]. D.Testa et al., Phys. Plasmas **6** (1999), 3498.
[14]. F.Rimini et al., Nucl. Fusion **39** (1999), 1591.
[15]. D.Testa et al., Review Scientific Instruments **74** (2003), 1694.
[16]. D.Testa et al., Phys. Plasmas **9** (2002), 243.
[17]. J.Noterdaeme et al., Nucl. Fusion **43** (2003), 274.
[18]. L.-G.Eriksson et al., submitted for publication in Phys. Rev. Lett., October 2003.
[19]. A.Fasoli et al., Phys. Plasmas **7** (2000), 1816.
[20]. L.Chen, Phys. Plasmas **1** (1994), 1519.
[21]. G.Vlad et al., submitted for publication in Plasma Phys. Control. Fusion, November 2003.

[22]. T.Stix, Nuclear Fusion **15** (1975), 737.
[23]. D.Testa, A.Fasoli, Nucl. Fusion **41** (2001), 809.
[24]. W.Heidbrink et al., Plasma Phys. Control. Fusion **45** (2003), 983.
[25]. F.Wagner et al., Phys. Rev. Lett. **49** (1982), 1408.
[26]. W.Suttrop et al., Plasma Phys. Control. Fusion **39** (1997), 2051.
[27]. Y.Andrew et al., submitted to Plasma Phys. Control. Fusion, November 2003.
[28]. A.Fasoli et al., Phys. Rev. Lett.**75** (1995), 645.
[29]. A.Jaun et al., Plasma Phys. Control. Fusion **43** (2001), A207.
[30]. J.Graves et al., Plasma Phys. Control Fusion **42** (2000), 1049.
[31]. R.Fitzpatrick, A.Aydemir, Nucl. Fus. **36** (1996), 11.
[32]. D.Ernst et al., Phys Plasmas **7** (2000), 615.

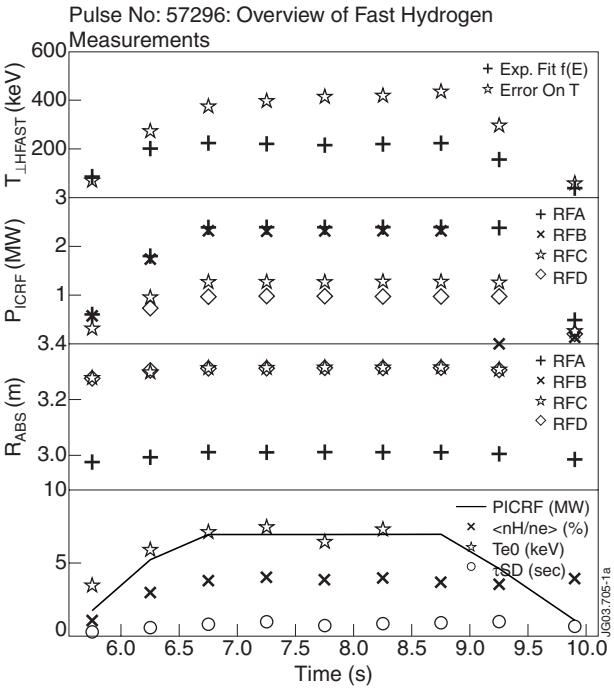

Figure 1: (a) NPA measurement of $T_{\perp HFAST}$ for Pulse No: 57296, the case of polychromatic ICRF heating. The four ICRF generators (RFA, RFB, RFC and RFD) operate at four different frequencies to spread the power deposition profile over $\Delta R_{ABS} \approx 50$cm. Here τ_{SD} and $<n_H>$ are the fast ion slowing down time and volume average hydrogen density, respectively.

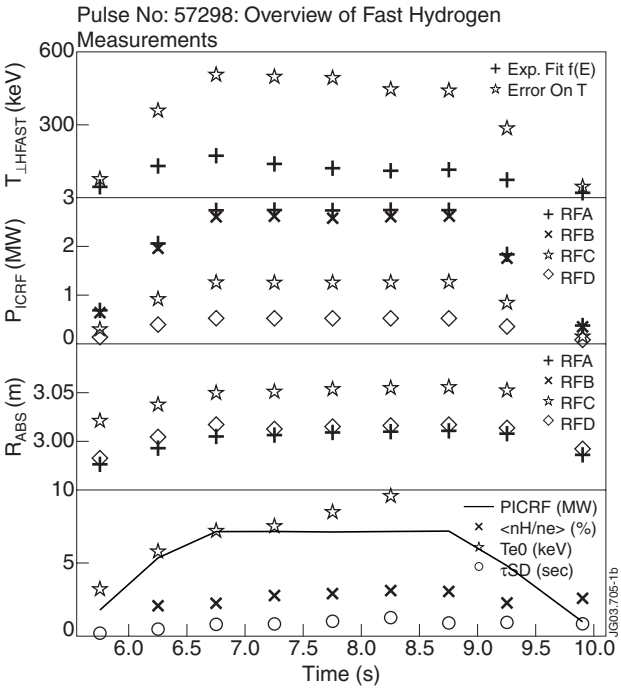

Figure 1: (b) NPA measurement of $T_{\perp HFAST}$ for Pulse No:57298, the case of monochromatic ICRF heating. The four ICRF generators operate at the same frequency to give a power deposition profile peaked on axis with a half-width at half-maximum of the order of $\Delta R_{ABS} \approx 25$cm.

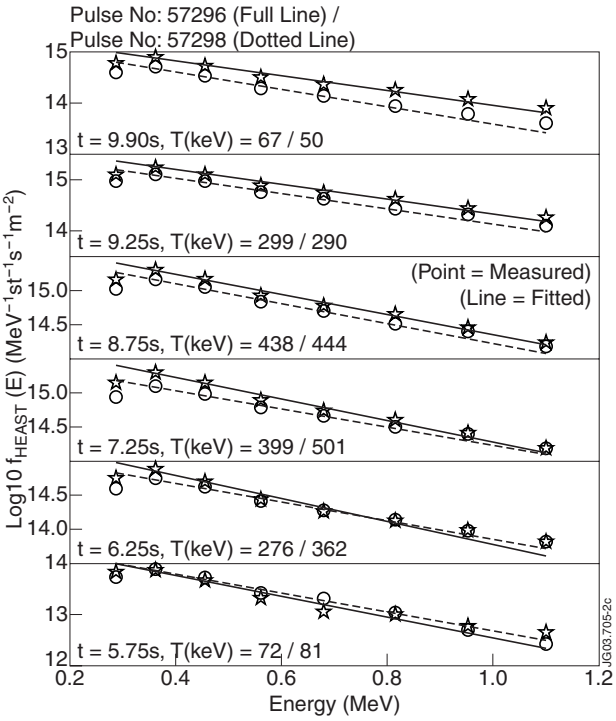

Figure 2: Measurement of the minority hydrogen distribution function for Pulse No's: 57296 and 57298, integrated along the line of sight of the high energy NPA.

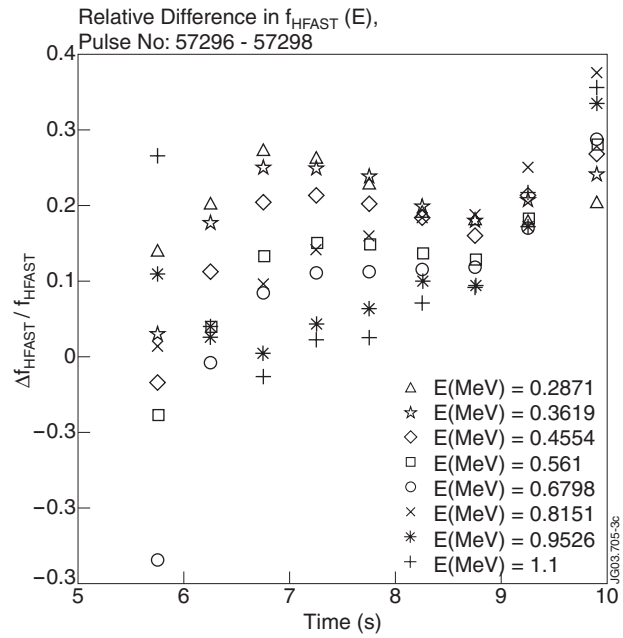

Figure 3: Relative difference in the measured $f_{HFAST}(E)$ between Pulse No's: 57296 and 57298.

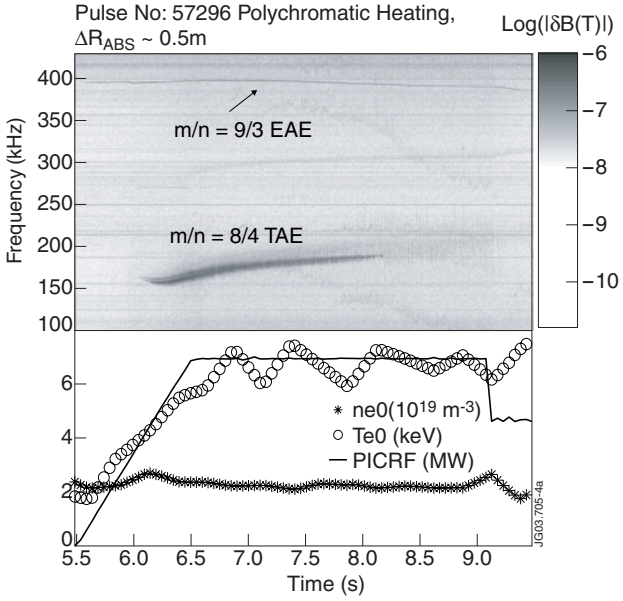

Figure 4: (a) Measurement of the mode activity in the Alfvén frequency range for Pulse No: 57296, the case of polychromatic ICRF heating.

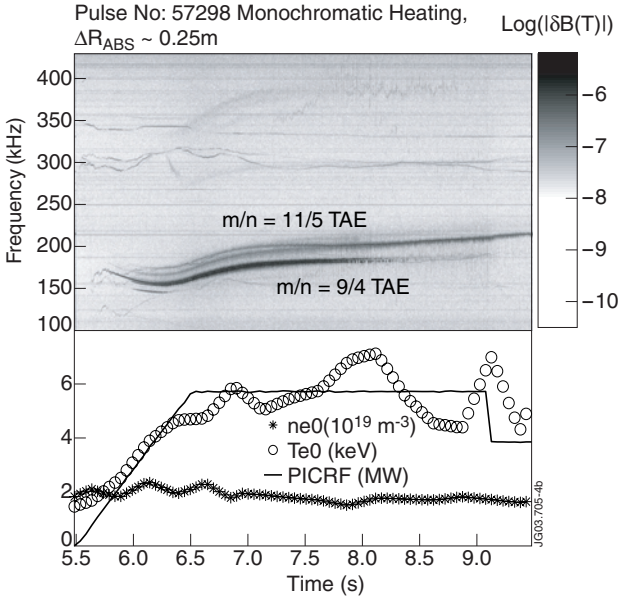

Figure 4: (b) Measurement of the mode activity in the Alfvén frequency range for Pulse No: 57298, the case of monochromatic ICRF heating.

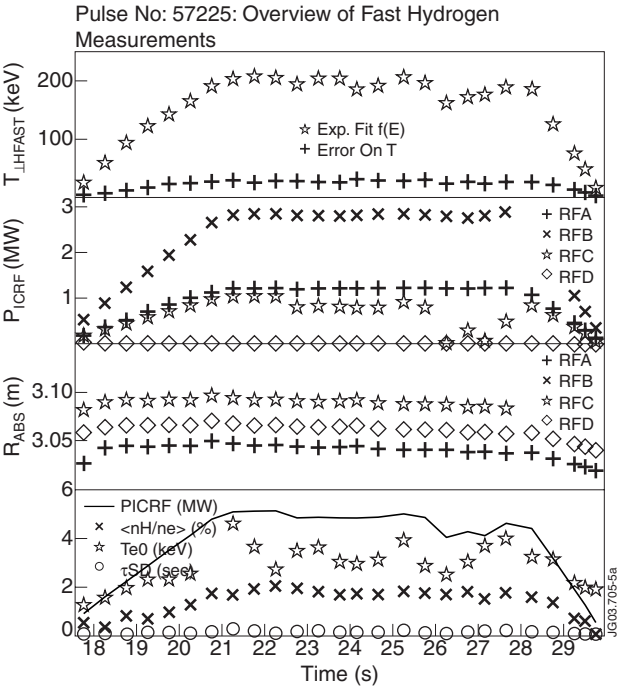

Figure 5: (a) Measurement of $T_{\perp HFAST}$ for Pulse No: 57225, the case of a low plasma density, $n_{e0} \approx 3 \times 10^{19} m^{-3}$.

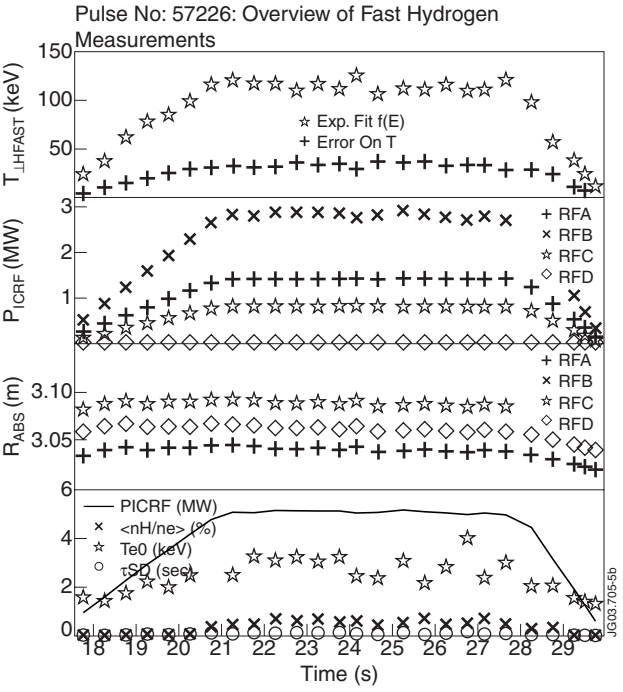

Figure 5: (b) Measurement of $T_{\perp HFAST}$ for Pulse No: 57226, the case of a high plasma density, $n_{e0} \approx 4 \times 10^{19} m^{-3}$.

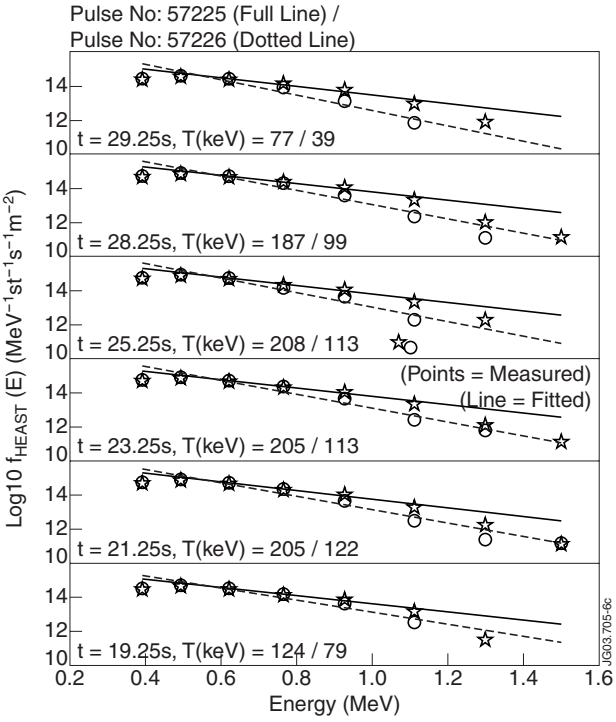

Figure 6: Measurement of the minority hydrogen distribution function for Pulse No's: 57225 and 57226, integrated along the line of sight of the high energy NPA.

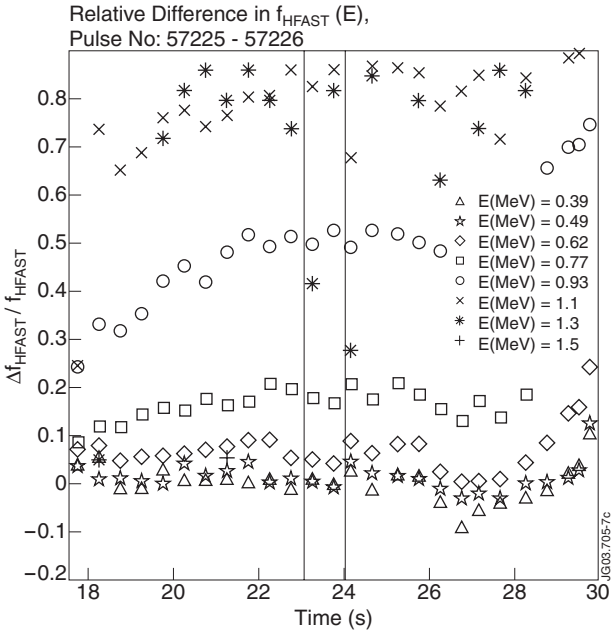

Figure 7. Relative difference in the measured $f_{HFAST}(E)$ between Pulse No's: 57225 and 57226. The vertical lines indicate two sawteeth in Pulse No: 57225, causing a significant reduction in $f_{HFAST}(E)$ at E>1.3MeV.

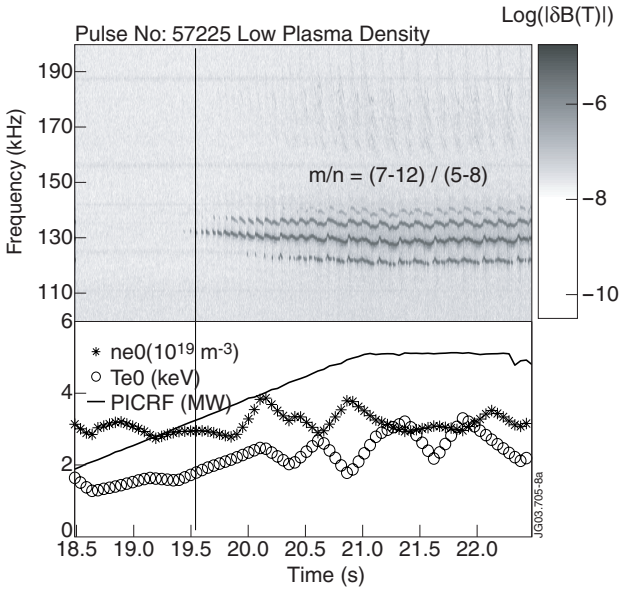

Figure 8:(a) Measurement of the mode activity in the Alfvén frequency range for Pulse No: 57225, the case of lower plasma density, $n_{e0} \approx 3\times10^{19}m^{-3}$, and higher fast ion temperature, $T_{\perp HFAST} \approx 200keV$.

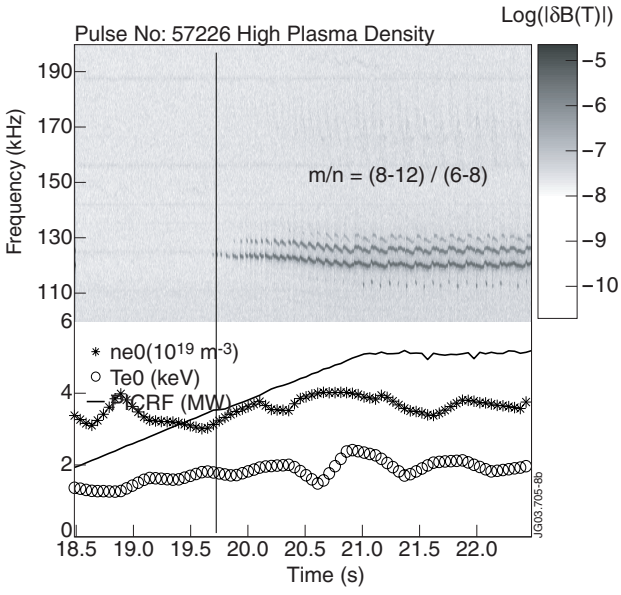

Figure 8:(b) Measurement of the mode activity in the AlfvÈn frequency range for Pulse No: 57226, the case of higher plasma density, $n_{e0} \approx 4\times10^{19}m^{-3}$, and lower fast ion temperature, $T_{\perp HFAST} \approx 120keV$.

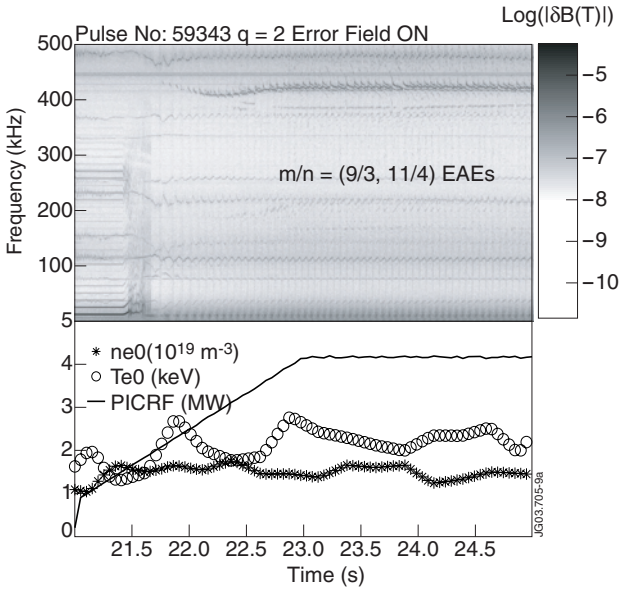

Figure 9:(a) Magnetic fluctuation spectrum for a discharge with externally induced low-amplitude error fields, which cause the formation of a q=2 magnetic island. Note the absence of TAEs around 180kHz, and the presence of $q_{EAE} \approx 3$ almost continuos EAEs around 400kHz.

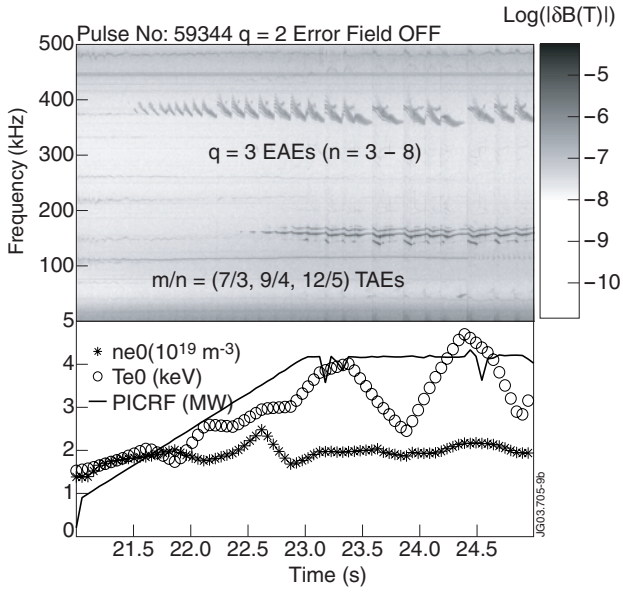

Figure 9:(b) Magnetic fluctuation spectrum for a discharge without the error fields, as in Fig.9a. Note the $q_{TAE} \approx 2$ TAEs around 180kHz, and the $q_{EAE} \approx 3$ chirping down EAEs around 400kHz.

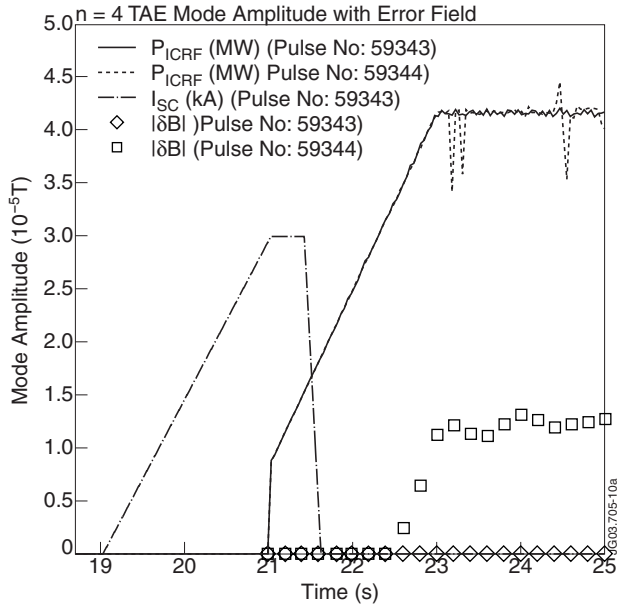

Figure 10:(a) Measurement of n = 4 TAE mode amplitude as function of P_{ICRF}. No mode is observed with the error fields, whereas without the error fields, the mode becomes unstable at $P_{ICRF} \approx 3$MW, and during the ICRF flat-top phase reaches the amplitude at the plasma edge $|\delta B|_{TAE} \approx 1.3 \times 10^{-5}$T.

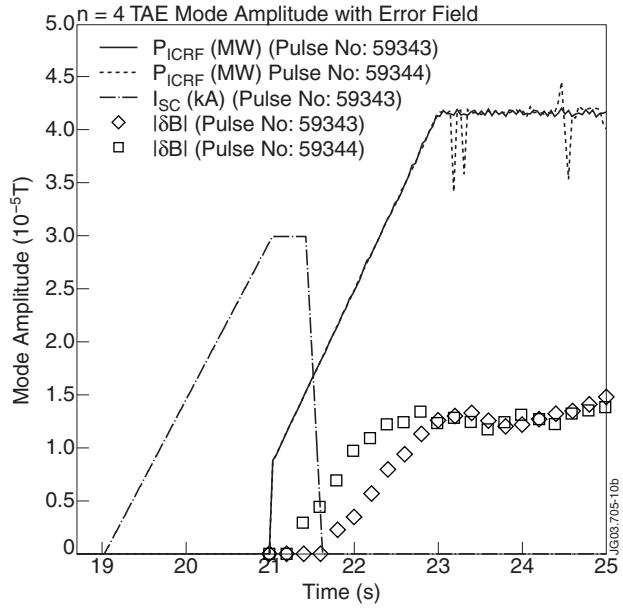

Figure 10:(b) Measurement of n = 4 EAE mode amplitude as function of P_{ICRF}. The only difference observed when the error fields are applied is the higher P_{ICRF} excitation threshold, $P_{ICRF} \approx 1.1$MW without the error fields compared to $P_{ICRF} \approx 2$MW with the error fields. During the ICRF flat-top phase, the mode reaches in both cases the amplitude at the plasma edge $|\delta B|_{TAE} \approx 1.4 \times 10^{-5}$T, very similar to $|\delta B|_{TAE}$ (Fig.10a).

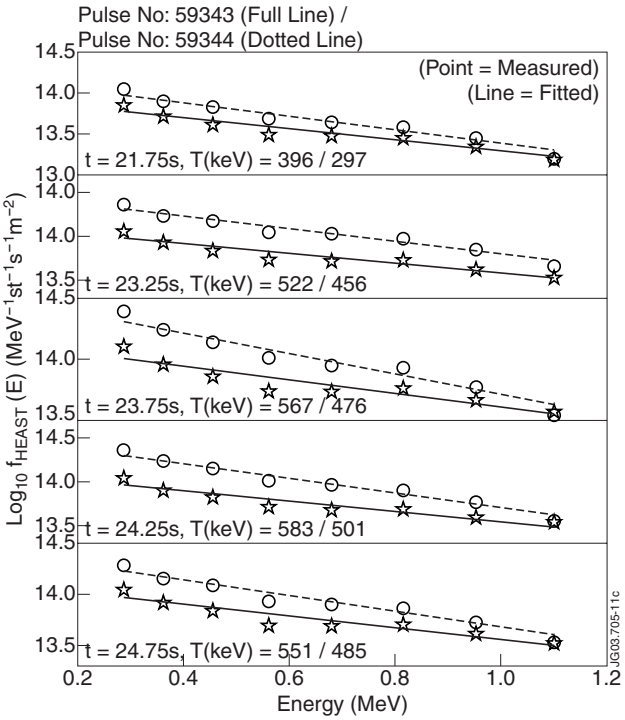

Figure 11: Measurement of the minority hydrogen distribution function for Pulse No's: 59343 and 59344, integrated along the line of sight of the high energy NPA.

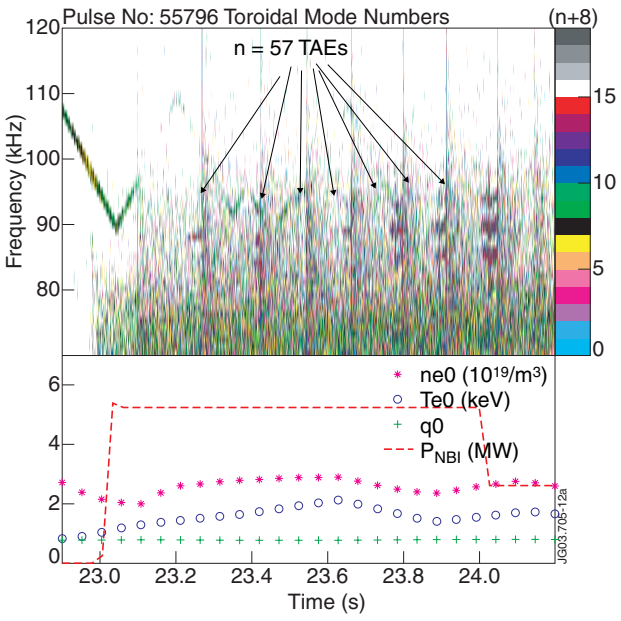

Figure 12:(a) Limiter plasma with monotonic q-profile and low edge magnetic shear: $n = 5 \div 7$ TAEs become unstable at $P_{NBI} = 5.3MW$, with $max(\upsilon_{||NBI}) \approx 0.8\upsilon_A$.

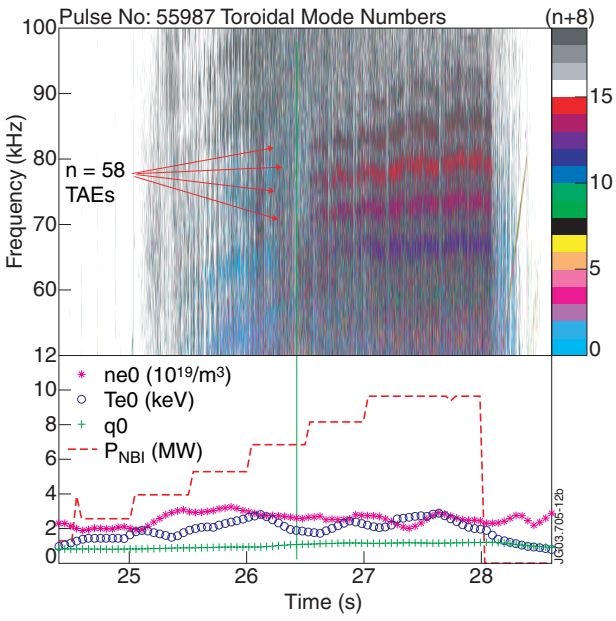

Figure 12:(b) X-point plasma with monotonic q-profile and high edge magnetic shear: $n = 5 \div 8$ TAEs become unstable at $P_{NBI} = 8MW$, with $max(\upsilon_{||NBI}) \approx 0.95\upsilon_A$.

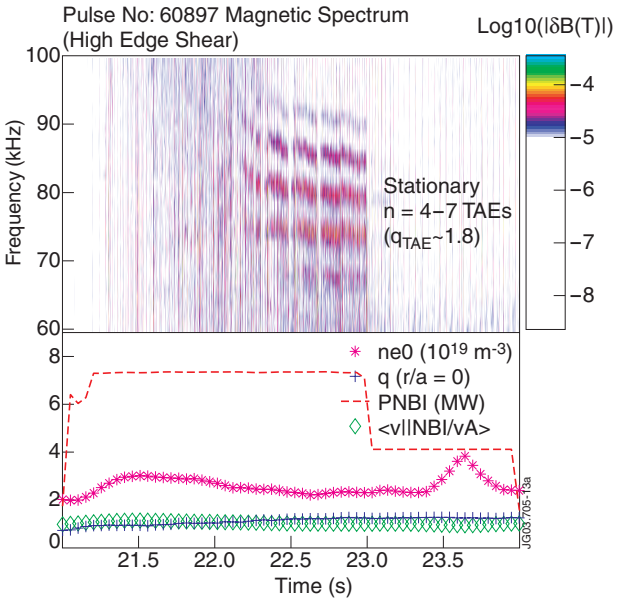

Figure 13: (a) X-point plasma with monotonic q-profile and high edge magnetic shear: n = 4÷7 TAEs located around the q~1.8 surface become unstable at P_{NBI} = 7.6MW, with max ($\upsilon_{||NBI}$) ≈ 1.05υ_A, and are clearly in a quasi steady-state regime.

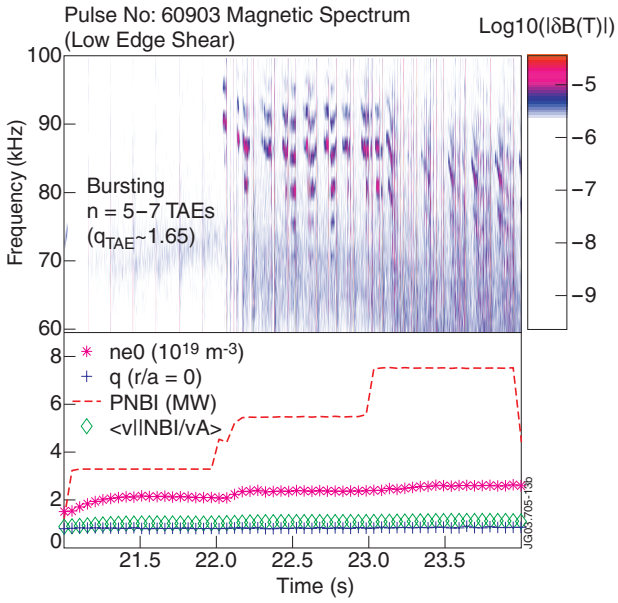

Figure 13: (b) Limiter plasma with monotonic q-profile and low edge magnetic shear: n = 5÷7 TAEs located around the q~1.65 surface become unstable at P_{NBI} = 5.6MW, with max ($\upsilon_{||NBI}$) ≈ 1.05υ_A.

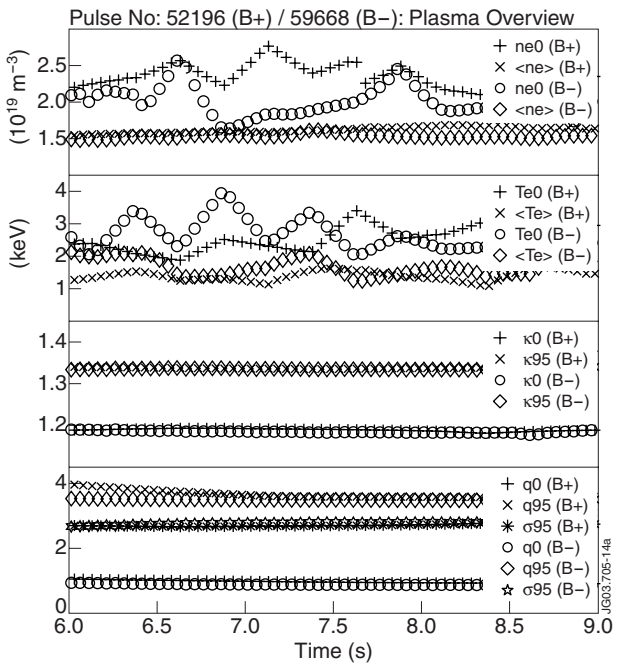

Figure 14: (a) Main plasma parameters for Pulse No: 52196 and 52198. Here κ_0 and κ_{95} are the elongation on axis and at 95% of the radius (similarly for the safety factor q_0 and q_{95} and the magnetic shear s_{95}).

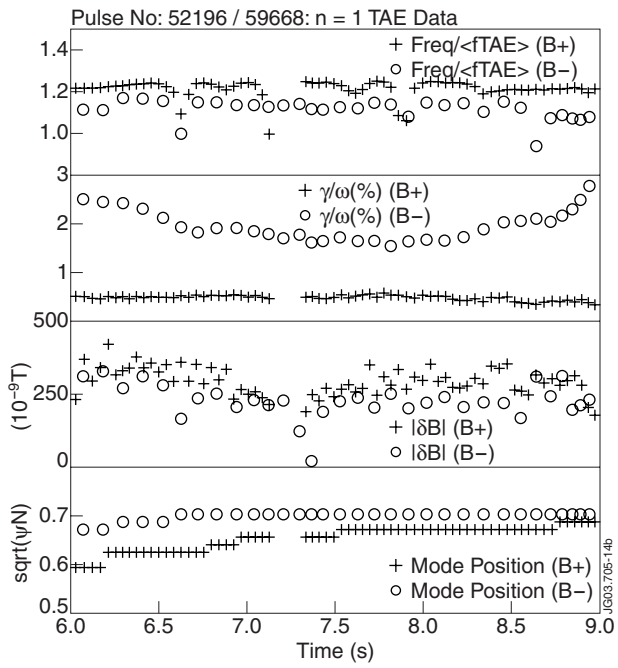

Figure 14: (b) Measurement of the frequency, damping rate, mode amplitude and radial position for n=1 TAEs as function of the ion ∇B-drift direction in plasmas with low-edge magnetic shear. Here <f_{TAE}> is the volume averaged TAE frequency.